Effect of nuclear motion on the absorption spectrum of dipicolinic acid

Petra Sauer, Yuri Rostovtsev, and Roland E. Allen
Department of Physics, Texas A&M University, College Station, Texas 77843

(Received 7 August 2006; accepted 21 November 2006; published online 11 January 2007)

Using semiclassical electron-radiation-ion dynamics, the authors have examined the effect of nuclear motion, resulting from both finite temperature and the response to a radiation field, on the line broadening of the excitation profile of 2,6-pyridinedicarboxylic acid (dipicolinic acid). With nuclei fixed, there is a relatively small broadening associated with the finite time duration of an applied laser pulse. When the nuclei are allowed to move, the excitation spectrum exhibits a much larger broadening, and is also reduced in height and shifted toward lower frequencies. In both cases, the excitation is due to well-defined π to π^* transitions. The further inclusion of thermal motion at room temperature broadens the linewidth considerably because of variations in the molecular geometry: Transitions that had zero or negligible transition probabilities in the ground state geometry are weakly excited at room temperature. © *2007 American Institute of Physics*. [DOI: 10.1063/1.2423017]

I. INTRODUCTION

A current scientific challenge is the rapid detection of chemical and biological substances, including bacterial spores. The inhalation of as few as 2500–55 000 *bacillus anthracis* spores is estimated to be lethal for approximately 50% of the exposed population, and infection may be caused by as few as one to three spores.[1] A variety of spectroscopic detection schemes are being explored, including fluorescence spectroscopy,[2,3] ultraviolet, and visible resonant Raman spectroscopy,[4,5] and a femtosecond adaptive spectroscopic technique using coherent anti-Stokes Raman scattering.[6] A significant component of the spores is the molecule dipicolinic acid (DPA) (or 2,6-pyridinedicarboxylic acid) and its salts.[5,7] This molecule has been shown to comprise between 5% (Ref. 8) and 15% (Ref. 9) of the spore coat, depending on environmental factors. DPA is a natural choice as a marker molecule since it has been found only in bacterial spores, and not in other common spores such as pollen or mold.[10]

Experimentally, the absorption spectra of aqueous solutions of DPA and its salts show several interesting features.[11] The calcium salt of DPA (CaDPA) has two closely spaced peaks at 271 and 278 nm, and a less well-defined region around 263 nm. The spectrum of DPA^{2-} (DPA with two protons removed) has only one clearly defined peak at 272 nm. The spectrum of DPA is the least well defined, with a maximum approximately at 270 nm. In each case, the spectra span wavelengths roughly from 250 to 290 nm.

A theoretical understanding of this absorption spectrum may provide important information for the further development of spore detection techniques. To our knowledge the only previous computational analysis of the excited state transitions of DPA consists of a time-dependent density-functional theory (TDDFT) study of both DPA and its dianion, DPA^{2-}, in gas phase, in water, and in ethanol.[12] The TDDFT calculations qualitatively captured several essential features of the experimental absorption spectrum. In these calculations, the first singlet excited state, a transition from highest occupied molecular orbital (HOMO) to lowest unoccupied molecular orbital (LUMO), is dipole forbidden. The first dipole-allowed transition occurs at a wavelength of 298 nm (for gas-phase DPA) but has a very weak oscillator strength (0.0013). The next two singlet excited state transitions are dipole forbidden. Excited states 5 and 6, occurring at 246 and 231 nm, are both dipole allowed and have significant oscillator strengths (0.0723 and 0.0919, respectively). These two closely spaced excitations, artificially broadened to mimic temperature and environmental factors, were compared to the experimental spectra with reasonable agreement.[12]

TDDFT calculations predict only the location, strength, and orbital symmetries of electronic transitions for specific geometrical configurations. Spectral broadening must be added artificially. (In both theory and experiment, the effects of homogeneous and inhomogeneous broadening are often invoked without a detailed analysis.) More realistic models should include nuclear motion, which affects the spectrum in many ways. For example, there is a qualitative change in the electronic excitations when the ground state symmetries are broken, and previously forbidden transitions may acquire nonzero oscillator strength. It is especially important to explore these effects in a molecule, such as DPA, that has a large number of negligible transitions in the ground state geometry for a specific polarization of the applied radiation field.

II. COMPUTATIONAL METHODS

Here we consider the response of DPA to laser pulses with various frequencies and durations. Since the time-dependent Schrödinger equation must be solved with a time step of ~1 as, it would be prohibitive to use any fully quantum method for a series of simulations with this relatively large molecule. We therefore employ semiclassical electron-radiation-ion dynamics (SERID), a technique that has been

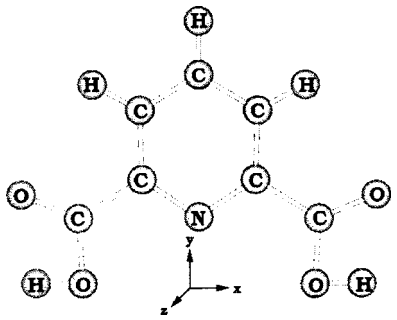

FIG. 1. Ground state geometry of DPA.

described in detail elsewhere,[13,14] and will be further clarified below. The time-dependent Schrödinger equation for the valence electrons is solved in a nonorthogonal basis at each time step. The Hamiltonian matrix and overlap matrix and the effective ion-ion repulsion are determined by parameters that derive from those originally fit to density-functional calculations.[15] Recently we have devised a simple scaling scheme that extends the original pairwise parameters for carbon and hydrogen to systems containing nitrogen and oxygen: The Hamiltonian matrix elements are scaled to reproduce the most relevant energy gap as calculated with DFT, and the effective repulsive potential is then scaled to reproduce the experimental bond lengths and vibrational frequencies.[16] The new parameters were tested on a set of polyatomic reference molecules and the results were found to be in reasonable agreement with experiment. The bond lengths are typically within 1%–3% of the experimental values, and never in error by more than 5%, for a variety of molecules with different geometries and bonding.

We have also previously used SERID with these parameters to study the details of the ground state geometry (see Fig. 1), molecular orbital structure, and allowed transitions in DPA.[16] All bond lengths were found to be within 5% of those calculated with DFT. The equilibrium molecular orbital energies near the HOMO-LUMO gap are summarized in Table I, for both the SERID and TDDFT calculations. In both calculations, there are three nearly degenerate occupied molecular orbitals separated by the HOMO-LUMO gap from two nearly degenerate unoccupied molecular orbitals. The lowest-energy excitation observed, from HOMO−2 to LUMO, was achieved only with *x*-polarized light. (The coordinate system is defined in Fig. 1.) The next excitation, from HOMO−2 to LUMO+1, was found to occur only with *y*-polarized light. There were no excitations out of either the HOMO or HOMO−1 levels for either polarization. Although there are slight differences in the *ordering* of the molecular orbitals near the HOMO-LUMO gap, the SERID and TDDFT calculations are in agreement concerning the *character and symmetry* of the orbitals involved in each transition.[16] We did not observe the transition from n to π (excited state 2 in the TDDFT calculations), but this transition has a very small oscillator strength. The TDDFT calculations also yield dipole matrix elements for the transitions that are in agreement with the polarizations described above for the SERID simulations.

TABLE I. Molecular orbital energies and symmetries calculated with SERID and DFT [B3LYP/6-311G+(2*df*,2*pd*)] for the ground state geometry.

Level	SERID (eV)	B3LYP (eV)	SERID symmetry	B3LYP symmetry
HOMO-3	−7.79	−8.82	π, B_1	π, B_1
HOMO−2	−7.20	−8.19	π, A_2	σ, B_2
HOMO−1	−7.05	−8.09	n, A_1	π, A_2
HOMO	−6.89	−7.67	σ, B_2	n, A_1
LUMO	−2.86	−2.37	π, B_1	π, A_2
LUMO+1	−2.59	−2.24	π, A_2	π, B_1

In the present approach, the radiation field is coupled to the electrons through the Peierls substitution[13]

$$H_{ab}(\mathbf{X}-\mathbf{X}') = H^0_{ab}(\mathbf{X}-\mathbf{X}')\exp\left(\frac{iq}{\hbar c}\mathbf{A}\cdot(\mathbf{X}-\mathbf{X}')\right), \quad (1)$$

where $\mathbf{A}$ is the vector potential, $q=-e$, and $\mathbf{X}$ is a nuclear position. We can then monitor the intricate relationship between nuclear motion and electron dynamics, as a laser pulse is applied with a given frequency, time duration, fluence, and polarization.

In the present context, it is particularly important to give a precise definition of the term "semiclassical" as it relates to the nuclear motion. Let us begin with Ehrenfest's theorem[14]

$$M\frac{d^2\hat{X}}{dt^2} = -\frac{\partial\mathcal{H}}{\partial\hat{X}} \quad (2)$$

where $\hat{X}$ is any nuclear coordinate, M is the corresponding mass, and $\mathcal{H}$ is the full Hamiltonian for all particles in the molecule. If the electrons are treated in a time-dependent self-consistent field picture, and the one-electron wave functions are represented in terms of localized basis functions, as in (12) and (15) of Ref. 13, one then obtains

$$M\frac{d^2\hat{X}}{dt^2} = -\sum_j \mathbf{\Psi}_j^\dagger(t)\cdot\frac{\partial\overleftrightarrow{H}(t)}{\partial\hat{X}}\cdot\mathbf{\Psi}_j(t) - \frac{\partial U_{\text{rep}}}{\partial\hat{X}} \quad (3)$$

where the state vector $\mathbf{\Psi}_j$ contains the coefficients of the basis functions for electron j. Here $\overleftrightarrow{H}(t)$ is the one-electron Hamiltonian matrix (derived from the one-electron Hamiltonian operator in a localized basis) and U_{rep} represents the effective repulsion between nuclei, as described in, e.g., Ref. 13.

Since quantum fluctuations, in the present context, are typically smaller than 0.05 Å for C and smaller than 0.10 Å even for H, it is a reasonable approximation to expand in a Taylor series about the expectation value

$$\langle\hat{X}\rangle \equiv X, \quad (4)$$

$$\frac{\partial\overleftrightarrow{H}}{\partial\hat{X}} = \left[\frac{\partial\overleftrightarrow{H}}{\partial\hat{X}}\right]_{\hat{X}=\langle\hat{X}\rangle} + \left[\frac{\partial^2\overleftrightarrow{H}}{\partial\hat{X}^2}\right]_{\hat{X}=\langle\hat{X}\rangle}(\hat{X}-\langle\hat{X}\rangle) + O((\hat{X}-\langle\hat{X}\rangle)^2), \quad (5)$$

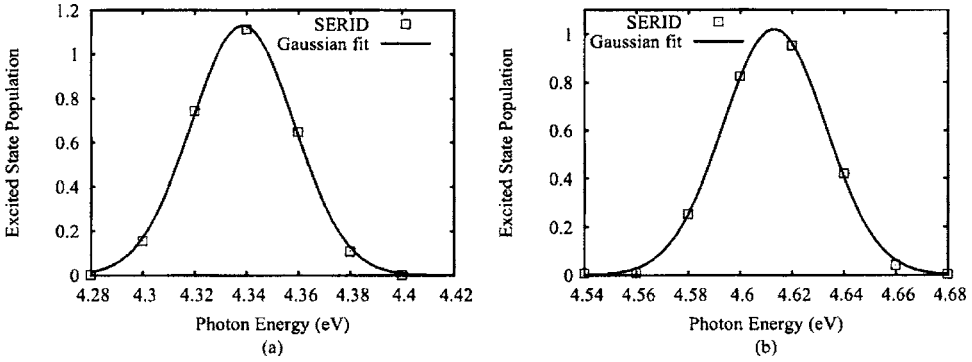

FIG. 2. (a) Results from SERID calculations (open squares), and a Gaussian fit to these results (solid line), for the excited state population following a laser pulse with a 25 fs half-width-at-half-maximum (HWHM) time duration and a fluence of 1.80×10^{-3} kJ/m^2, which is polarized in the x direction. (Parameters for the Gaussian fit: $\alpha_0=1.130$, $\hbar\omega_0=4.339$ eV, and $\hbar\Delta\omega=0.028$ eV.) (b) Results for a pulse with same frequency, duration, and fluence, but polarized in the y direction. (Parameters for the Gaussian fit: $\alpha_0=1.020$, $\hbar\omega_0=4.613$ eV, and $\hbar\Delta\omega=0.028$ eV.)

$$\frac{\partial U_{\mathrm{rep}}}{\partial \hat{X}} = \left[\frac{\partial U_{\mathrm{rep}}}{\partial \hat{X}}\right]_{\hat{X}=\langle\hat{X}\rangle} + \left[\frac{\partial^2 U_{\mathrm{rep}}}{\partial \hat{X}^2}\right]_{\hat{X}=\langle\hat{X}\rangle} (\hat{X}-\langle\hat{X}\rangle) + O((\hat{X}-\langle\hat{X}\rangle)^2), \tag{6}$$

and neglect the terms of order $(\hat{X}-\langle\hat{X}\rangle)^2$. Then taking the expectation value in Eq. (3) gives

$$M\frac{d^2X}{dt^2} = -\sum_j \mathbf{\Psi}_j^{\dagger}(t)\cdot\frac{\partial\vec{H}(t)}{\partial X}\cdot\mathbf{\Psi}_j(t) - \frac{\partial U_{\mathrm{rep}}}{\partial X}. \tag{7}$$

A cavalier (although usually adequate) definition of the semiclassical approximation would simply state that the operator $\hat{X}$ of Eq. (3) is replaced by a classical variable X. But now we can see what the proper definition really is [for the semiclassical approximation which takes us from Eq. (3) to Eq. (7)]. We merely neglect the quantum fluctuations in $\partial\vec{H}/\partial\hat{X}$ and $\partial U_{\mathrm{rep}}/\partial\hat{X}$; i.e., we assume that we can discard all but the leading two terms in each Taylor series expansion about $\hat{X}=\langle\hat{X}\rangle$. In this approximation, Eq. (7) then gives the time evolution of $\langle\hat{X}\rangle$.

This fact is particularly important in the present context because the motion considered in this paper is the motion of *the expectation value* $\langle\hat{X}\rangle$. In our calculations the motion due to quantum fluctuations of the nuclear positions never appears because it has already been averaged out.

The physical effects that we will consider are also not influenced by the quantum fluctuations, but are instead associated with the time evolution of $\langle\hat{X}\rangle$, which results from either thermal motion or the response to a laser pulse. As will be shown below, the largest effect is the breaking of initial symmetries in the ground state, permitting previously forbidden transitions to occur. This symmetry breaking results from the changes in $\langle\hat{X}\rangle$ for the various nuclear coordinates within the molecule.

The quantum fluctuations *within* a molecular state are not directly relevant because we are concerned with the transitions *between* molecular states. To say it in a different way, the electronic states and the allowed transitions are determined primarily by $\langle\hat{X}\rangle$, and this is the quantity that we calculate.

We conclude this discussion by mentioning that there are situations in which the quantum fluctuations are important: namely, experiments which effectively measure the positions or velocities of the nuclei. For example, an x-ray diffraction experiment effectively measures the distribution of positions (as seen in the Debye-Waller factor for a crystal) and nuclear reactions effectively measure the distribution of velocities (as seen in Doppler broadening). But we are concerned with transition energies rather than positions or velocities. This distinction is already clear in a classical treatment of a harmonic oscillator, where the position and velocity vary with time, but the energy does not. Similarly, quantum fluctuations do not broaden the energy of the molecular eigenstate.

III. RESULTS AND DISCUSSION

A. Excitation spectrum with frozen nuclei

We first performed simulations in which the nuclei were frozen in place, in the sense that $\langle\hat{X}\rangle$ was fixed for each coordinate $\hat{X}$, in order to verify quantitatively that the line broadening in this case results only from the finite time duration of the pulse (which implies a width for the frequencies of the allowed transitions according to the time-energy uncertainty relation). Broadening of the excitation spectrum means that radiation with frequencies near but not exactly equal to the resonant frequency for a given transition will still produce excitation. We therefore performed simulations for laser pulses whose frequencies were varied over a range corresponding to photon energies between 4.28 and 4.68 eV, in increments of 0.02 eV. In each simulation the pulse had a half-width-at-half-maximum (HWHM) duration of 25 fs and a fluence of 1.80×10^{-3} kJ/m^2. (This fluence was chosen so that the maximum excited state population was close to one electron.) In Fig. 2 the excited state population at the end of each laser pulse is shown as a function of photon energy for both x- and y-polarized light. The uncertainty principle suggests that the width of the spectrum should be $\sim\hbar/\Delta t$, so a linewidth of about 0.026 eV is expected for this pulse duration. As a test of this idea and the calculations, we have fitted the excited state population data obtained from the simulations to a Gaussian function of the form

$$\alpha(\omega) = \alpha_0 e^{-((\omega-\omega_0)/\Delta\omega)^2}.$$

For both polarizations, the linewidth $\hbar\Delta\omega$ is 0.028 eV, in very good agreement with the expected value. As mentioned previously, these SERID transitions also agree quite well

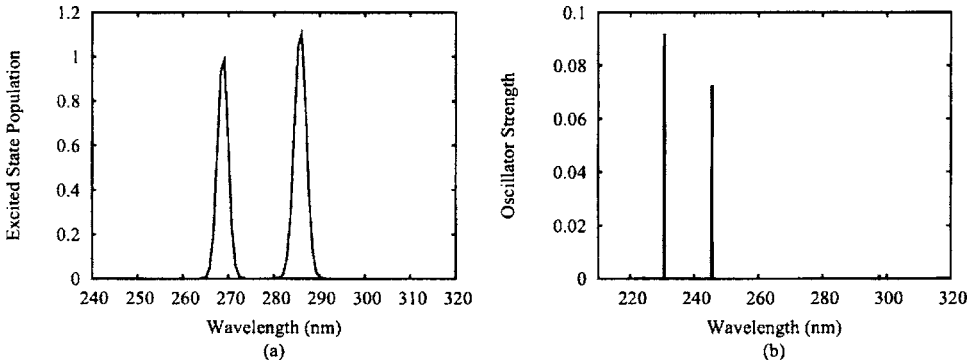

FIG. 3. Gaussian fit to (a) the excited state population vs wavelength, as calculated with SERID, and (b) the oscillator strength vs wavelength, as calculated with TDDFT.

with the TDDFT calculations. For each polarization, the transitions are from π to π^* orbitals of similar symmetry. The first significant transition calculated with SERID occurs at 286 nm, for *x*-polarized light. The second occurs at 269 nm, for *y*-polarized light. Although the two methods show quantitative differences in the position of the peaks, the spacing between the two peaks is similar (17 nm for SERID versus 15 nm for TDDFT). A comparison of the Gaussian fits to the excited state population versus wavelength for *x* and *y* polarizations, as calculated with SERID, and of the oscillator strength versus wavelength, as calculated with TDDFT, is shown in Fig. 3. The location of these peaks is in reasonable agreement with the experimental absorption spectra, which show a broad peak near 270 nm.[11]

B. Effect of nuclear motion with initial temperature of 0 K

The present method (SERID) includes the interaction between nuclear motion and electron dynamics, an effect that is of critical importance in the present context. In this section we permit nuclear motion, but start the molecule at a temperature of 0 K, so that the nuclear motion is solely due to forces induced by electronic excitation. The predominant motion of the nuclei, during the full 100 fs duration of the laser pulse, is a relaxation to slightly elongated bond lengths together with the initiation of oscillatory motion. The response of a typical carbon-carbon ring bond is shown in Fig. 4. The best Gaussian fit to the excited state population shows that there is a slight broadening of the linewidth, but that there are also four other substantial effects when the nuclear response is included, as can be seen in Fig. 5: (1) a decrease in the strength of the response, (2) a shift to lower frequencies, (3) a plateau region at higher frequencies, and (4) an abrupt cutoff at low frequency.

The first effect results from the modification of the electronic energy levels as the nuclear positions change, so that the photon energy is no longer matched to the difference in relevant electronic energies (in this case, the HOMO−2 and LUMO levels) for the full duration of the laser pulse.

The remaining three effects are similarly due to changes in the electronic energy levels which result from changes in the molecular geometry. These changes in geometry are determined by the occupancies of the excited states, which are in turn dependent on the frequency of the applied laser pulse. The fact that the shift in electronic energy levels is different for different photon energies—i.e., different frequencies—is demonstrated in Fig. 6. As the electronic population increases in the excited states, geometrical changes occur that tend to decrease the energy difference between the HOMO −2 and LUMO levels. There is then a positive feedback loop which produces a redshift in excitation energies (effect 2 above). This alteration of the time-averaged electronic levels, expressed as a function of the photon energy associated with the applied laser pulse, also explains the plateau region at higher frequencies: In this region, there is only a small occupation of the excited states, inducing very little nuclear motion, and the electronic energy levels remain out of resonance with the frequency of the applied laser pulse. Between 4.35 and 4.40 eV, therefore, one has a plateau with little excitation (effect 3 above). In the opposite regime of lower frequencies, there is a cutoff below which the photon energy

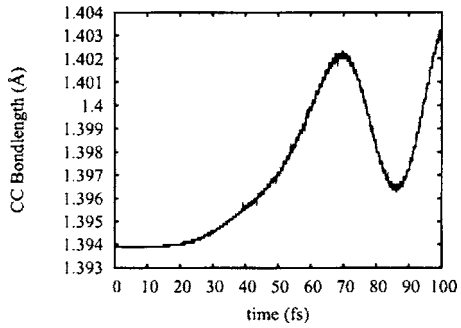

FIG. 4. Response of a typical carbon-carbon ring bond to a 25 fs (HWHM) pulse with a photon energy of 4.28 eV and a fluence of 1.80×10^{-3} kJ/m^2, polarized in the *x* direction, during a 0 K simulation.

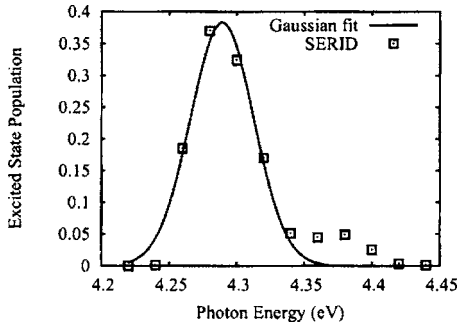

FIG. 5. Excited state population as a function of laser pulse photon energy, for simulations involving a 25 fs (HWHM) pulse with a fluence of 1.80×10^{-3} kJ/m^2 polarized in the *x* direction. The parameters determined by the Gaussian fit are $\alpha_0=0.383$, $\hbar\omega_0=4.289$ eV, and $\hbar\Delta\omega=0.033$ eV.

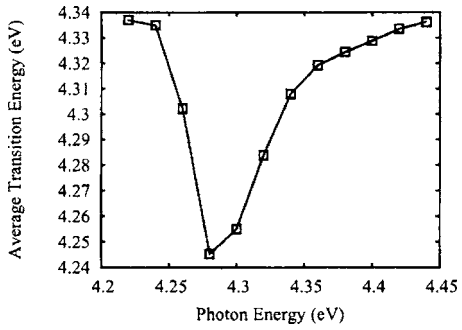

FIG. 6. Difference in most relevant time-averaged electronic energy levels (HOMO−2 and LUMO of Table I) as a function of photon energy for simulations with a 25 fs (HWHM) pulse having a fluence of 1.80×10^{-3} kJ/m^2 and polarized in the x direction.

is insufficient to produce any appreciable excitations. As a result there is also no nuclear motion. One observes this abrupt cutoff in Fig. 5 (effect 4 above).

One expects all these effects of nuclear motion to be more pronounced at higher intensities, and this is confirmed by the results of Fig. 7, where the fluence was increased to 4.5×10^{-3} kJ/m^2. It is clear that there is a broadening of the excitation spectrum, and an enhancement of the asymmetrical features of the absorption peak, at this higher laser pulse intensity. The abrupt cutoff for redshifted energies remains in the vicinity of 4.24 eV, but exhibits a more sharply defined on/off behavior.

C. Effect of nuclear motion at 300 K

In the simulations of the preceding section, the molecule initially had all the symmetries of the ground state geometry. As a consequence, the excitation features described above are associated with a single transition from HOMO−2 (π,A_2) to LUMO (π,B_1) with x-polarized light or HOMO −2 (π,A_2) to LUMO+1 (π,A_2) with y-polarized light. There were no excitations out of either the HOMO (σ,B_2) or HOMO−1 (n,A_1) levels. For x-polarized light there was no excitation to the LUMO+1 level and for y-polarized light there was no significant excitation into the LUMO level.

Let us now turn to simulations at finite temperature. The atoms in the molecule are assigned random initial velocities, $d\langle\hat{X}\rangle/dt$, which are then reduced and scaled so that the total momentum is zero and the total kinetic energy is equal to $(3N-3)kT/2$, where N is the number of atoms, k is the Boltzmann constant, and T is the temperature. We first calculated the excited state population for a 25 fs (HWHM) laser pulse with fluence of 1.80×10^{-3} kJ/m^2, polarized in the x direction. The response to the laser pulse of both a typical carbon-carbon ring bond and a carbon-hydrogen bond is shown in Fig. 8. The carbon-carbon bond oscillates with a period of approximately 20 fs, permitting about five complete oscillations during the full 100 fs duration of the laser pulse. The carbon-hydrogen bond has a period of roughly 10 fs, allowing about ten full oscillations during application of the laser pulse. The oscillation amplitudes for the carbon-carbon and carbon-hydrogen bonds are about 0.04 and 0.02 Å, respectively. As can be seen in Fig. 9, the response of the electrons

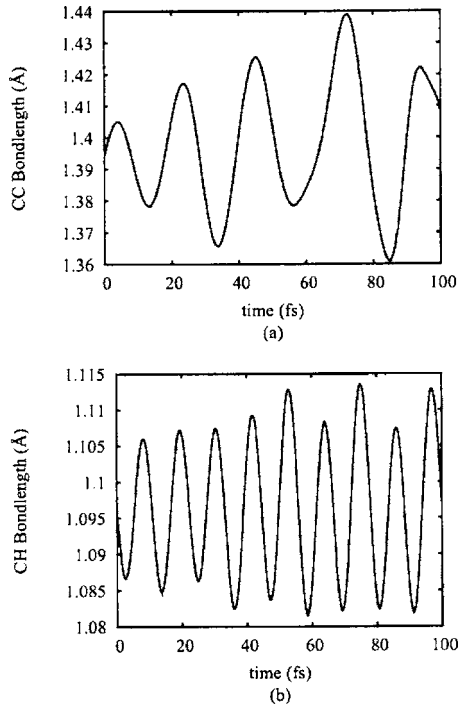

FIG. 8. Response of (a) a typical carbon-carbon ring bond and (b) a typical carbon-hydrogen bond to a 25 fs (HWHM) pulse with a photon energy of 4.28 eV and a fluence of 1.80×10^{-3} kJ/m^2, polarized in the x direction, during a room temperature simulation.

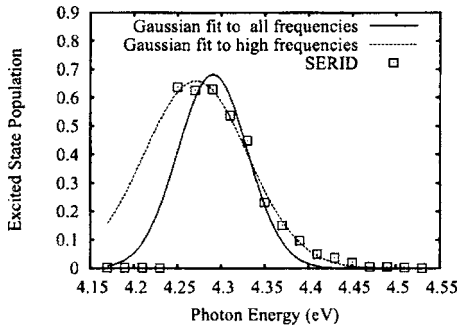

FIG. 7. Excited state population vs laser photon energy for a 25 fs (HWHM) pulse with fluence of 4.5×10^{-3} kJ/m^2 polarized in the x direction. Parameters for a Gaussian fit to all the data are $\alpha_0=0.681$, $\hbar\omega_0=4.290$ eV, and $\hbar\Delta\omega=0.056$ eV. Parameters for a Gaussian fit to data points with energies higher than 4.24 eV are $\alpha_0=0.657$, $\hbar\omega_0=4.271$ eV, and $\hbar\Delta\omega=0.084$ eV.

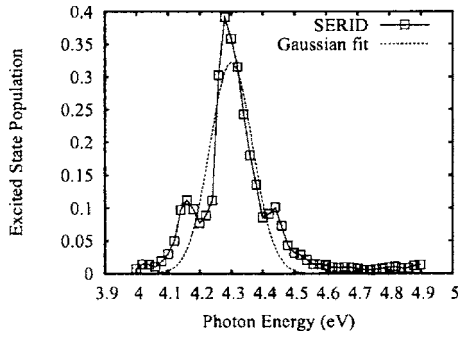

FIG. 9. Excited state population vs photon energy for a 25 fs (HWHM) pulse with fluence of 1.80×10^{-3} kJ/m^2 polarized in the x direction. In these simulations and those of the following figures, the molecule was initially at a temperature of 300 K. Parameters for a Gaussian fit to the data are $\alpha_0=0.323$, $\hbar\omega_0=4.301$ eV, and $\hbar\Delta\omega=0.095$ eV.

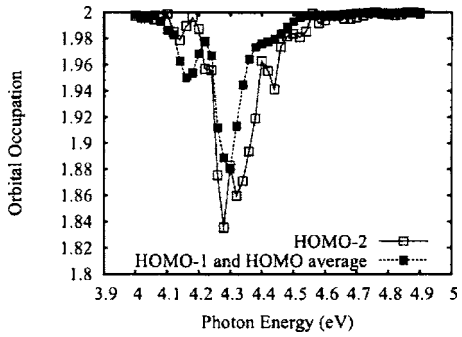

FIG. 10. Occupation of the HOMO, HOMO−1, and HOMO−2 states as functions of photon energy for a 25 fs (HWHM) pulse with a fluence of 1.80×10^{-3} kJ/m^2, polarized in the x direction.

is characterized by a main peak centered at about 4.30 eV, which is still due to the primary excitation from HOMO−2 to LUMO, but there is a small side peak on either side. Both the plateau region and the abrupt cutoff seen earlier in the zero temperature simulations are now dominated by the more prominent sideband effects. The width of the Gaussian fit to the results (for excited state population versus photon energy) is approximately three times that obtained in the case of frozen nuclei.

Since the linewidth of the zero temperature simulations at this fluence was only slightly larger than that for frozen nuclei, we attribute the broadening primarily to excitations in the sidebands, which were previously not allowed by the ground state symmetries of the molecule. Figure 10 depicts the occupation of the HOMO−2 orbital and the average occupation of the HOMO and HOMO−1 orbitals, as functions of photon energy for the room temperature simulations. Recall that the zero temperature simulations showed excitation from only the HOMO−2 state (to the LUMO), and did not show any depopulation of either the HOMO−1 or HOMO states, even though the HOMO−2, HOMO−1, and HOMO are closely spaced in energy. The room temperature simulations for photon energies at about 4.2 eV, on the other hand, show excitations out of the HOMO−1 and HOMO states (and not the HOMO−2). This is the reason for the redshifted sideband in this frequency range, which can be seen in Fig. 10.

The blueshifted sideband has a different origin, which is revealed by Fig. 11: The populations of the LUMO and LUMO+1 levels are shown as functions of time for a pulse with a photon energy of 4.44 eV (in the center of the blueshifted sideband). Recall that the zero temperature simulations showed no occupancy of the LUMO+1 state even though the LUMO and LUMO+1 are closely spaced. In the room temperature simulations for this photon energy, on the other hand, both the LUMO and the LUMO+1 levels become occupied, with the electronic population alternating between these two levels as a function of time.

In summary, the sidebands for the room temperature simulations result from transitions that are either forbidden or negligibly small in the ground state molecular geometry. The sideband that is redshifted from the central absorption peak is caused by excitations out of both the HOMO and HOMO−1 orbitals and the blueshifted sideband is due to excitations into the LUMO+1 orbital.

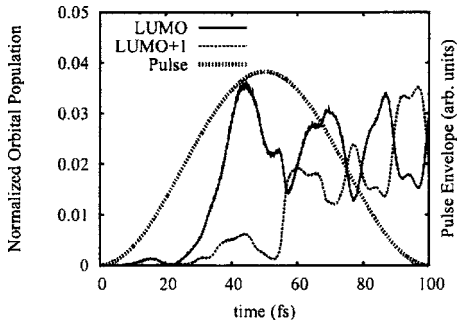

FIG. 11. LUMO and LUMO+1 occupancies as functions of time for a room temperature simulation of a 25 fs (HWHM) pulse with a fluence of 1.80×10^{-3} kJ/m^2 and photon energy of 4.44 eV, polarized in the x direction. The laser pulse envelope (thick dashed line) is also shown, plotted in arbitrary units.

IV. CONCLUSIONS

In Fig. 12, our results are compared for three cases: no nuclear motion (i.e., $d\langle\hat{X}\rangle/dt=0$); nuclear motion resulting only from response to the laser pulse, with the molecule initially in its ground state; and nuclear motion resulting both from thermal effects at 300 K and from the response to the applied laser pulse. In each case the DPA molecule was subjected to x-polarized laser pulses having a fluence of 1.80×10^{-3} kJ/m^2 and a duration of 25 fs (HWHM).

These results demonstrate that the nuclear motion tends to decrease, broaden, and redshift the excitation spectrum.

An additional issue is the effect of lower occupied and higher unoccupied electronic states (which, respectively, lie below the HOMO, HOMO−1, and HOMO−2 states or above the LUMO and LUMO+1 states discussed above). In our simulations with y-polarized light at room temperature, we find that the central transition is due to excitations from HOMO−2 to LUMO+1 states, but, as can be seen in Fig. 13, there is a linear rise in the excited state population at large photon energies. This effect represents the onset of the next large excitation peak, which is produced by depopulation of orbitals lower in energy than the HOMO−2 state. This feature, observed in our SERID simulations, is also predicted with a large oscillator strength in the TDDFT calculations. In order to attempt an accurate Gaussian fit to the data, we have subtracted off this effect in the results displayed below. Even when this effect of the deeper occupied states is

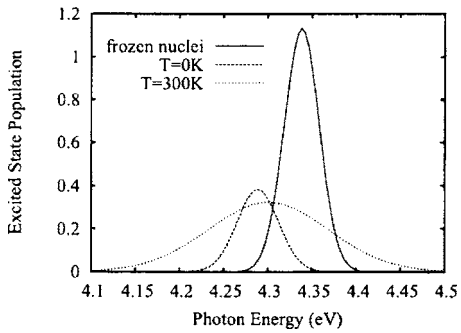

FIG. 12. Comparison of Gaussian fits to the results of SERID simulations for all three cases: frozen nuclei, molecule initially in ground state geometry, and molecule initially at room temperature.

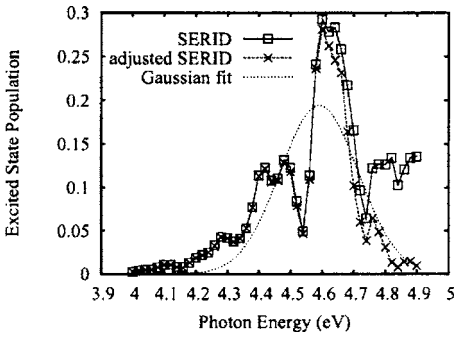

FIG. 13. Excited state population vs photon energy for 25 fs (HWHM) pulse with fluence of 1.80×10^{-3} kJ/m^2, polarized in the y direction. The adjusted spectrum is derived from the original results (for a simulation with the molecule initially at room temperature) by removing excitations out of orbitals lying lower than the HOMO−2 state. Parameters for a Gaussian fit to the data are $\alpha_0=0.194$, $\hbar\omega_0=4.591$ eV, and $\hbar\Delta\omega=0.175$ eV.

substracted out, however, the width of the peak is still substantially broader than for the simulations in which the nuclei were frozen.

In order to provide a rough comparison between our SERID results for laser pulses and the experimental results of Ref. 11 for cw light, we have added the x- and y-polarized Gaussian fits to obtain (in terms of wavelength)

$$\alpha(\lambda) = 0.10e^{-((\lambda - 270.1)/10.29)^2} + 0.16e^{-((\lambda - 288.3)/6.43)^2}.$$

This result of this average over polarizations is shown in Fig. 14, together with the actual results of the SERID room temperature simulations for x-polarized light, y-polarized light, and light polarized at an angle of 45° with respect to each axis. The total width of the broad double-peaked region is approximately 40 nm, comparable to the linewidths of the experimental absorption spectra of Ref. 11. (Only the contribution from thermal motion is relevant in comparing with these cw experiments, but, as can be seen in Fig. 12, this is the dominant contribution.) These results therefore indicate that a large amount of the observed line broadening is due to nuclear motion within the molecule, and not just effects of the inhomogeneous environment.

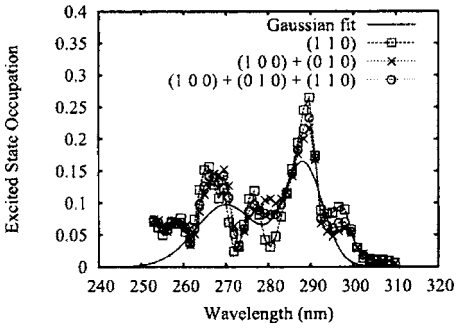

FIG. 14. Excited state population vs laser pulse wavelength for room temperature simulations of a DPA molecule subjected to a 25 fs (HWHM) laser pulse with a fluence of 1.80×10^{-3} kJ/m^2, with several polarizations, as described in the text and labeled in the figure.

In summary, our simulations demonstrate that nuclear motion leads to substantial broadening of the excitation spectrum of DPA because variations in the molecular geometry permit excitations that are not allowed in the ground state geometry: There are three rather closely spaced occupied states near the HOMO-LUMO gap and two unoccupied states that are also relatively close in energy. In the ground state molecular geometry, most transitions between these states are either dipole forbidden or have very small oscillator strength. When the motion of the nuclei is included, many of these forbidden or very weak transitions become stronger, resulting in sidebands on either side of the main absorption peaks. A Gaussian fit to the single molecule profile, used to represent an average over many molecules with different initial conditions, shows a spectrum that is much broader than that obtained with no nuclear motion.

ACKNOWLEDGMENTS

This work was supported by the Robert A. Welch Foundation (Grant No. A-0929), the Defense Advanced Research Projects Agency, and the Office of Naval Research (Award No. N00014-03-1-0385). The authors would like to thank K. K. Lehmann, R. Lucht, R. Murawski, Z. E. Sariyanni, M. O. Scully, J. Reintjes, and J. R. Xie for many helpful discussions. One of the authors (P.S.) thanks the Supercomputing Facility at Texas A&M University for the use of its parallel supercomputing capabilities.

[1] T. V. Ingleslby, T. O'Toole, D. A. Henderson *et al.*, J. Am. Med. Assoc. **287**, 2236 (2002).
[2] A. Alimova, A. Katz, H. E. Savage, M. Shah, G. Minko, D. V. Will, R. B. Rosen, S. A. McCormick, and R. R. Alfano, Appl. Opt. **42**, 4080 (2003).
[3] S. Sarasanandarajah, J. Kunnil, B. V. Bronk, and L. Reinisch, Appl. Opt. **44**, 1182 (2005).
[4] D. Pestov, M. Zhi, Z. Sariyanni *et al.*, Proc. Natl. Acad. Sci. U.S.A. **102**, 14976 (2005).
[5] E. Ghiamati, R. Manoharan, W. H. Nelson, and J. F. Sperry, Appl. Spectrosc. **46**, 357 (1992).
[6] M. O. Scully, G. W. Kattawar, R. P. Lucht, T. Opatrny, H. Pilloff, A. Rebane, A. V. Sokolov, and M. S. Zubairy, Proc. Natl. Acad. Sci. U.S.A. **99**, 10994 (2002).
[7] W. H. Woodruff, T. G. Spiro, and C. Gilvarg, Biochem. Biophys. Res. Commun. **58**, 197 (1974).
[8] J. J. Perry and J. W. Foster, J. Bacteriol. **69**, 337 (1955).
[9] J. F. Powell and R. E. Strange, Biochem. J. **54**, 205 (1953).
[10] S. Farquharson, L. Grigely, V. Khitrov, W. Smith, J. F. Sperry, and G. Fenerty, J. Raman Spectrosc. **35**, 82 (2004); See also, S. Farquharson, W. Smith, C. Brouillette, and F. Inscore, Spectroscopy, June 2, 2005, published online at http://www.spectroscopymag.com/spectroscopy/article/articleDetail.jsp?id=166430
[11] R. Nudelman, B. V. Bronk, and S. Efrima, Appl. Spectrosc. **54**, 445 (2000).
[12] J. R. Xie, V. H. Smith, and R. E. Allen, Chem. Phys. **322**, 254 (2006).
[13] Y. Dou, B. R. Torralva, and R. E. Allen, J. Mod. Opt. **50**, 2615 (2003).
[14] R. E. Allen, Phys. Rev. B **50**, 18629 (1994), Eq. (13). See also the equation above, Eq. (4) in Ref. 13.
[15] D. Porezag, Th. Frauenheim, Th. Koehler, G. Seifert, and R. Kaschner, Phys. Rev. B **51**, 12947 (1995).
[16] P. Sauer and R. E. Allen, J. Mod. Opt. **53**, 1619 (2006).